Separation and Purification Technology 286 (2022) 120466

Contents lists available at ScienceDirect

Separation and Purification Technology

journal homepage: www.elsevier.com/locate/seppur

Zero-valent iron-copper bimetallic catalyst supported on graphite from spent lithium-ion battery anodes and mill scale waste for the degradation of 4-chlorophenol in aqueous phase

Shuai Chen [a,b], Fei Long [a], Guilan Gao [a,*], Carolina Belver [b], Zixiang Li [a], Zhuoxiang Li [a], Jie Guan [a], Yaoguang Guo [a], Jorge Bedia [b,*]

[a] Research Center of Resource Recycling Science and Engineering, School of Environmental and Materials Engineering, Shanghai Polytechnic University, Shanghai 201209, China

[b] Chemical Engineering Department, Facultad de Ciencias, Universidad Autonoma de Madrid, Campus Cantoblanco, Madrid E-28049, Spain

ARTICLE INFO

Keywords:
Zero-valent iron-copper
Heterogeneous Fenton
Reduction
Advanced oxidation
4-chlorophenol

ABSTRACT

Graphite supported zero-valent iron-copper bimetallic catalysts (ZVI-Cu/C) were successfully prepared from mill scale (MS) waste and spent lithium-ion battery (LIB) anode using carbothermic reduction as a new approach for the recycling and revalorization of these waste. Cu and graphite were obtained from the LIB anodes, while ZVI was provided by MS waste. ZVI-Cu/C were synthesized with different MS to LIB anode powers mass ratios (1 to 4) and used as catalysts for the degradation of 4-chlorophenol (4-CP) in water by both reduction and heterogeneous Fenton reactions. ZVI-Cu/C-2 showed the highest removal percentage of 4-CP in both reactions. The degradation rates fitted well to a pseudo first-order model for both reactions. Moreover, ZVI-Cu/C-2 catalyst showed a relatively low lixiviation of iron and copper ions and a high activity in the 4-CP removal even in the fourth reuse cycle, which supports the high stability of the synthesized catalyst. Hydroquinone and 4-chlorocatechol were identified as the main intermediate by-products of 4-CP degradation. The results of this study support the possibility of synthesizing high active and stable ZVI-Cu/C catalysts using graphite and copper from spent LIB anode and iron oxide from MS waste. These catalysts show promising prospective for the removal of 4-CP in water, with comparable activities to others previously reported. This study reports, for the first time, the combined recycling of MS waste and spent LIB anodes to synthesize ZVI-Cu/C catalysts for water treatment by both oxidation and reduction reactions.

1. Introduction

Lithium-ion batteries (LIBs) have been rapidly developed and widely used since early 1990s in portable electronic products, medical instruments, military facilities, electric energy storage systems and electric vehicles. They possess advantages in terms of high specific energy, stable discharge voltage, small self-discharge, long service life and no memory effect [1]. In 2020, 500,000 tons of spent LIBs were generated in China, and it is estimated that the number of spent LIBs worldwide, from 2017 to 2030, will exceed 11 million tons [2]. The data of the U.S. Geological Survey shows that at most only 20% of those spent LIBs are recycled [3], while the report of the International Resources Panel shows that the recycled LIBs in the world are less than 1% [4]. Leakage of cobalt, nickel and other heavy metals, and release of lithium hydrate, from these spent LIBs, can pollute water resources [5,6]. In addition, China, which produces more than 50% of the world's LIBs, will face a serious shortage of raw materials due to the rapid growth of their demand and the almost constant annual mining amount [7]. However, spent LIBs contain valuable materials including metals like lithium, cobalt and aluminum in the cathodes, as well as copper and graphite in the anodes. Therefore, effective recycling of spent LIBs can not only resolve their serious environmental problems of spent LIBs, but also avoid the waste of valuable and scarce resources. Nowadays, the research on spent LIBs recycling mainly focuses on the separation and purification of metals using pyrometallurgy and hydrometallurgy technologies [5,8]. Meanwhile, a few references reported interesting attempts on the employment of parts of spent LIBs to make materials for the elimination of contaminants. Niu et al. [9] synthesized a Li–Cl–Co

* Corresponding authors.
E-mail addresses: glgao@sspu.edu.cn (G. Gao), jorge.bedia@uam.es (J. Bedia).

https://doi.org/10.1016/j.seppur.2022.120466
Received 30 October 2021; Received in revised form 21 December 2021; Accepted 6 January 2022
Available online 10 January 2022
1383-5866/© 2022 The Author(s). Published by Elsevier B.V. This is an open access article under the CC BY-NC-ND license (http://creativecommons.org/licenses/by-nc-nd/4.0/).

anion–cation, from one-pot sintering at 530 °C of $LiCoO_2$ cathode, melamine and NH_4Cl, aimed to regulate the π-conjugated structure of g-C_3N_4 and to enhance its photocatalytic activity for photodegradation of rhodamine B in water. Liang et al. [10] synthesized magnetic $CoFe_2O_4$ from spent $LiCoO_2$ cathodes to activate peroxymonosulfate (PMS) for bisphenol A degradation in water. Similarly, Zhao et al. [11] reutilized $LiCoO_2$ cathode as a heterogeneous catalyst to remove antibiotics in wastewater via PMS activation. Zhang et al. [12] reused spent LIB cathodes as adsorbents for removal of aqueous heavy metals. Krishnasamy et al. [13] recycled graphite from the anode to convert electromagnetic energy into heat energy for soil remediation. These papers showed promising ways of transforming spent LIBs to functional materials for environmental applications. However, the simultaneous recycling of graphite and copper in the anodes has not been studied.

In addition, mill scale (MS), which is constituted mainly by iron oxides, is a hazardous steel waste generated in rolling mills from the intensive steel industry [14]. Around 40–60 kg of MS is generated per each steel ton [15]. According to the data from the Ministry of Industry and Information Technology of China, the steel production reached 1.325 billion tons in 2020, which underlines the great importance of recycling a so huge amount of MS waste. Bantsis et al. [16] used four kinds of Greek woods to mix with MS and obtained porous iron oxide ceramics that can be used for electromagnetic interference protection. Shahid et al. [17] pretreated and filtered MS with sulfuric acid, then added the remaining solids to sodium hydroxide to obtain magnetite for arsenic removal in water. Liu et al. [18] mixed MS with manganese ore and obtained iron manganese with a purity of 97.5% through sintering, grinding and magnetic separation. Jikar and Dhokey [19] pre-oxidized MS at 1100 °C, and reduced it with an hydrogen/nitrogen mixture to obtain iron powder. All these studies confirm the significance of the searching for alternatives for the recycling/reuse of MS waste. One of these alternatives is its use as precursor for iron-based high value products, such as zero valent iron (ZVI), which has shown a wide perspective in the removal of pollutants in water because of its high activity in the presence and absence of oxygen [20]. However, the iron (hydrogen) oxide passivation layer, generated by the reaction of ZVI with water on its surface, reduces the availability of active sites and hinders the electron transfer, thus reducing its reactivity [21]. The addition of small quantities of other metals, like copper, to ZVI, and using carbon materials as support can further improve its activity [22,23]. MS has a high iron content, a stable chemical composition, and a low percentage of impurities [24], making it an excellent and economical precursor for ZVI production. In addition, the higher ordering degree of graphite results in a better electrical conductivity than disordered activated carbons, and consequently it can be used as support to further improve the electron transport capacity and reactivity of the supported ZVI [25,26]. In our previous study [27], graphite loaded ZVI, synthesized through carbothermal reduction reaction of MS and graphite from spent LIB anodes, showed a promising behavior in the ibuprofen removal in water, with a good recycling ability and a very high stability under the reaction conditions with small amount of iron loss by lixiviation.

In this study, MS and ball milled spent LIB anodes are recycled to prepare graphite supported ZVI-Cu bimetallic (ZVI-Cu/C) catalysts. The effect of ball milling to the copper content in various particle sizes is studied to determine the optimal recycling strategy of the copper in spent LIB anodes. 4-chlorophenol (4-CP), a common toxic and refractory compound, was used as model pollutant to test the activity of ZVI-Cu/C catalysts in water both for reduction and heterogeneous Fenton reactions. Comparison of the 4-CP removal results of this study and the ones reported using reduction, photocatalytic degradation, biological elimination and heterogeneous Fenton processes were also made to discuss the application potential of these techniques [28–41]. To the best of our knowledge, this is the first study that recycles both LIB anodes and MS waste to synthesize ZVI-Cu/C catalysts through a single carboreduction step. These catalysts show significant activities in reduction and oxidation reactions of 4-CP degradation, besides to a high stability.

2. Materials and methods

2.1. Chemicals and materials

Hydrogen peroxide (H_2O_2, 30%) and 4-CP (>99%) were obtained from Sinopharm Chemical Reagent Co., Ltd. (Shanghai, China). Sunwoda (Shenzhen, China) 3349C1D spent LIBs were firstly discharged in NaCl solution (20 g/L) for 24 h and then manually dismantled to obtain their anodes. The anodes were cut into 1 × 1 cm fragments, mixed with the steel balls (5 mm in size) and fed into the Changsha Deke (Changsha, China) PBM-V-0.4L ball mill for 6 h at a speed of 600 rpm and with a ball to material ratio increasing from 80:1 to 100:1. The anode particles smaller than 0.15 mm were further used to synthesize ZVI-Cu/C composites, while the larger particles can be used to recycle the copper because of its higher content in this metal. MS was obtained from Baosteel (Shanghai, China), and the particles with size lower than 0.18 mm were used to prepare the catalysts.

2.2. Synthesis of ZVI-Cu/C catalysts

Spent LIB anode powders (0.5 g) with sizes smaller than 0.15 mm were physically mixed with 0.5, 1.0, 1.5 and 2.0 g of MS to synthesize ZVI-Cu/C-1, ZVI-Cu/C-2, ZVI-Cu/C-3 and ZVI-Cu/C-4, respectively, being the last number the mass ratio between the MS and the LIB anode powders. These mixtures were heated for 2 h at 1000 °C under N_2 atmosphere (120 $cm^3 \cdot min^{-1}$) in a Zhonghuan (Tianjin, China) SK-G06123K tubular furnace in ceramic crucibles. During the synthesis, the iron oxides in MS were reduced to ZVI through the carbothermic reactions showed in Eqs. (1)–(3) [27]. After this heating, the catalysts were characterized without additional treatments and tested as catalysts for water treatment.

$$3C + Fe_2O_3 \rightarrow 3CO\uparrow + 2Fe \quad (1)$$

$$3C + 2\,Fe_2O_3 \rightarrow 3CO_2\uparrow + 2Fe \quad (2)$$

$$3CO + Fe_2O_3 \rightarrow 3CO_2\uparrow + 2Fe \quad (3)$$

2.3. Characterization

The crystalline structure of all samples was characterized by X-ray diffraction (XRD) using a BRUKER AXS GMBH D8 diffractometer. The diffraction patterns were registered from 10° to 90° of 2θ in steps of 0.02° and 2 s counting time per step. The surface morphology was observed by Scanning Probe Microscope (SPM) and Transmission Electron Microscopy (TEM) using a Shimadzu SPM-9600 microscope and a JEOL JEM-1400 microscope (operated at the accelerating voltage of 120 kV), respectively. The elemental compositions were analyzed using EDAX TEAM Apollo Energy Dispersive Spectroscopy (EDS). The surface elements of ZVI-Cu/C were measured by the Kratos Axis Ultra DLD X-ray photoelectron (XPS) spectrometer that employs a monochromatic Al Kα X-ray source (hυ = 1486.6 eV). To analyze the XPS signal of elements, C1s peak position was fixed at 284.5 eV and used as internal reference. Peak deconvolution was performed using Gaussian–Lorentzian peak shapes using the least-squares method. Textural analyses of materials were analyzed by N_2 adsorption–desorption at −196 °C using a Micromeritics TriStar 123 static volumetric system. The samples were previously outgassed under vacuum at 150 °C for 2 h, and the specific surface area was estimated by the Brunauer–Emmett–Teller (BET) method. The content of metals in the aqueous solutions after reaction was quantified using a Thermo Fisher Scientific ICE3000 atomic absorption spectrometer (AAS).

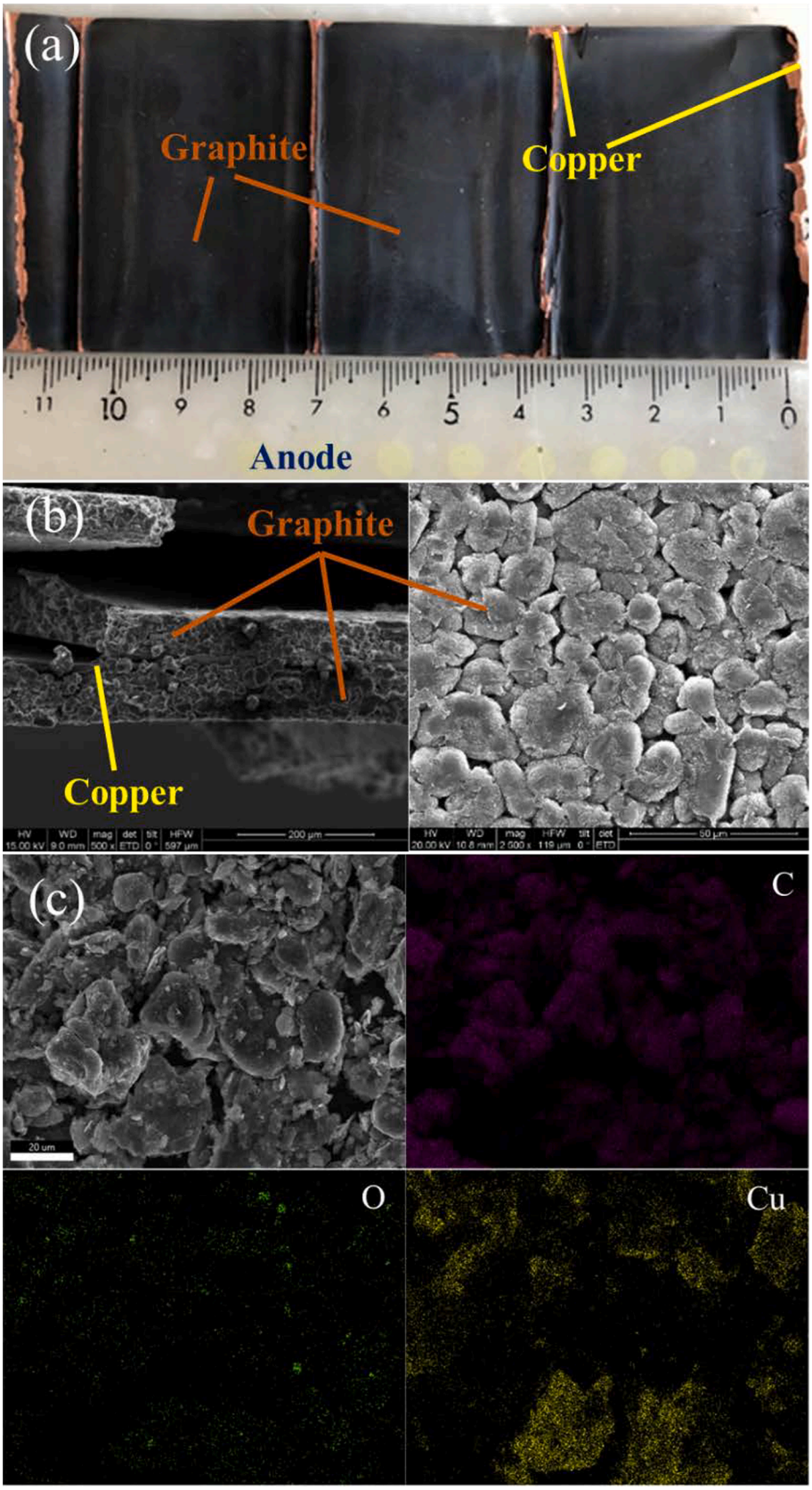

Fig.1. (a) Photograph and (b) SEM images of spent LIB anode and (c) SEM-EDS results of spent LIB anode after ball milling.

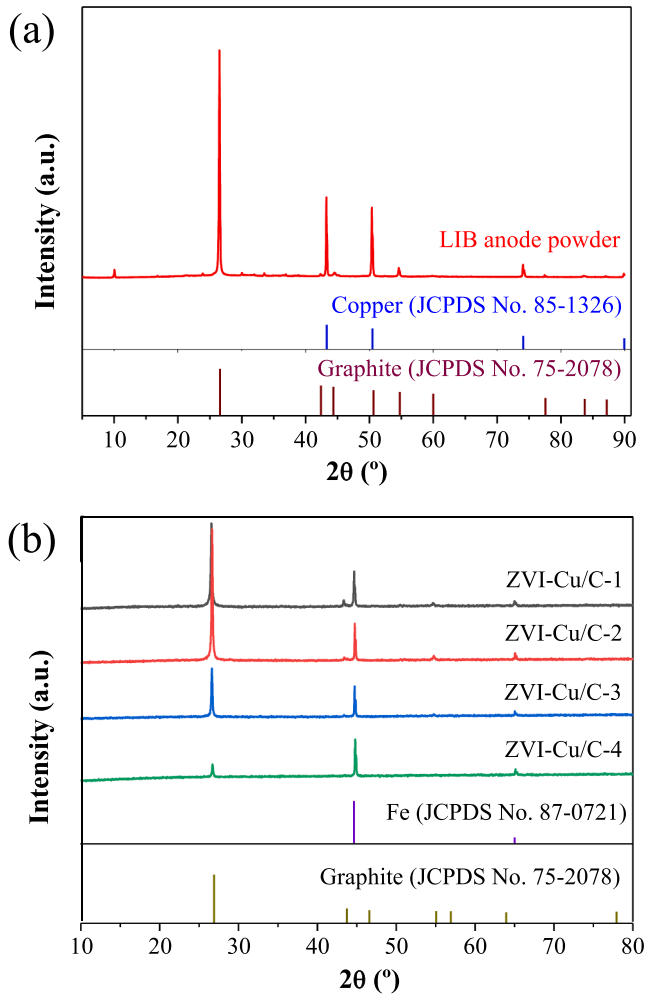

Fig. 2. (a) XRD patterns of spent LIB anode powders and (b) ZVI-Cu/C composites.

2.4. Degradation of 4-CP in water with ZVI-Cu/C composites

Degradation tests were all carried out in 250 mL flasks at 20 °C on a table concentrator (150 rpm) containing 100 mL of 4-CP solution (10 $mg{\cdot}L^{-1}$) and a concentration of ZVI-Cu/C of 0.2 $g{\cdot}L^{-1}$. For the heterogeneous Fenton tests (oxidation reaction), the H_2O_2 concentration was fixed at 0.5 mM, and the pH of the solution was adjusted at 3 with 0.1 M HCl solution. For the reduction tests, the pH of the solution was also adjusted to 3 with 0.1 M HCl solution but no H_2O_2 was added. At given time intervals, 2 mL of the solution were collected and analyzed by Liquid Chromatography (LC) with a Shimadzu LC-20 apparatus to determine the concentrations of 4-CP. The XBridgeC18 reversed phase column (4.6 mm × 250 mm × 5 μm), the UV–visible detector at the wavelength of 280 nm, the mobile phase of methanol and water ($V_{methanol}$: V_{water} = 6:4) at the flow rate of 1 $mL{\cdot}min^{-1}$, and the column temperature of 30 °C, and a injection volume of 20 μL were used. Gas chromatography-mass spectrometry (GC–MS; Agilent 8890-5977B) was used to quantify the concentrations of the reaction by-products formed during the 4-CP degradation processes, following the methods of USEPA 3510C-1996 and USEPA 8270E-2018. We have analyzed the catalyst stability in oxidation reaction. After each 4-CP removal cycle, the used ZVI-Cu/C catalysts were recovered and washed with deionized water 3 times, vacuum dried for 6 h, and reused in another cycle, adding 0.5 mM H_2O_2 and setting the pH to 3 in each cycle. All the experiments detailed above were performed by triplicate and the average values are reported.

Table 1
Size distribution and copper content of spent LIB anode powders after ball milling.

Ball/anode mass ratio	80	90	100	
Size (mm)	Mass ratio (%)	Mass ratio (%)	Mass ratio (%)	Coper content (%)
>0.25	20.3	20.2	16.8	41.8
0.18–0.25	4.9	2.9	2.9	0.6
0.15–0.18	9.2	0.8	0.6	0.7
0.1–0.15	30.3	31.5	31.4	0.9
0.075–0.1	22.5	28.1	26.5	0.9
0.05–0.075	4.6	11.4	13.0	0.8
<0.05	8.1	5.1	8.7	0.6

3. Results and discussion

3.1. Sieve analysis of spent LIB anode after ball milling

A photograph and SEM images of spent LIB anodes before ball milling are shown in Fig. 1a and b, respectively. The spent LIB anode is made up of an inner copper foil covered with smooth surface graphite on both sides. The SEM-EDS and XRD results of spent LIB anodes after ball milling are depicted in Fig. 1c and Fig. 2a, respectively. The copper foil and graphite layer in the spent LIB anode were destroyed during the milling. Mixed copper and graphite particles were obtained. This is confirmed the XRD pattern of the spent LIB powders and the EDS results, which show the presence of copper and carbon (this latter, from the graphite content) more or less homogeneously distributed.

Table 1 shows the size distributions of spent LIB anode powders after ball milling. As the mass ratio of ball to material in the milling processes increased from 80:1 to 100:1, the particles with sizes lower than 0.15 mm were gradually enriched, accounting for about 65–80% of the total. Moreover, the biggest particles (>0.25 mm) have a 41.8% of copper, which is much higher than the corresponding 7.7% for the non-milled spent LIB anode. This indicates that, after milling, the biggest particles suffer a copper enrichment, probably due to the higher ductility of copper than graphite, which can be very useful to facilitate the separation of copper for further recycling. For the synthesis of the different catalysts, we used a ball/anode mass ratio of 100 (which maximizes the amount of smaller particles) and the fraction with particle size lower than 0.15 mm, which showed a higher graphite content (obtained by difference) but with a low amount of Cu (an average of approximately 0.7%) that can improve the ZVI activity and stability [22].

3.2. Characterization of ZVI-Cu/C composites

The XRD patterns (Fig. 2a) of ZVI-Cu/C catalysts show the characteristic diffraction peaks of ZVI at 44.6° (JDPDS No. 87–0721), confirming that ZVI has been successfully synthesized during the carbothermal reduction. All patterns show the main graphite peak at 26° of 2θ (JDPDS No. 75–2078), whose intensity decreases considerably as the MS ratio increases. This can be due to the graphite consumption during the carbothermal reduction of the MS (see Eqs. (1) and (2)). The SEM-EDS images of ZVI-Cu/C-2 show ZVI and Cu particles deposited on the graphite surface (Fig. 3a). The TEM image of ZVI-Cu/C-2 shows that part of the metal particles is dispersed between the graphite layers. This type of bimetallic Fe-Cu combinations has previously shown higher activity than bare ZVI in the degradation of tetrabromobisphenol A, a persistent organic pollutant [22].

The characterization of ZVI-Cu/C-2 by XPS confirmed the presence of iron, copper and carbon at the surface. Fig. 4 represents the Fe 2p, Cu 2p and C 1 s XPS deconvoluted spectra. Only a very weak peak of $Fe2P_{3/2}$ at about 706 eV was detected, most likely because this technique has a low penetration depth (<3 nm) and because of the presence of the oxidation shell (Fe^{3+}) covering the core ZVI that limits the access of the

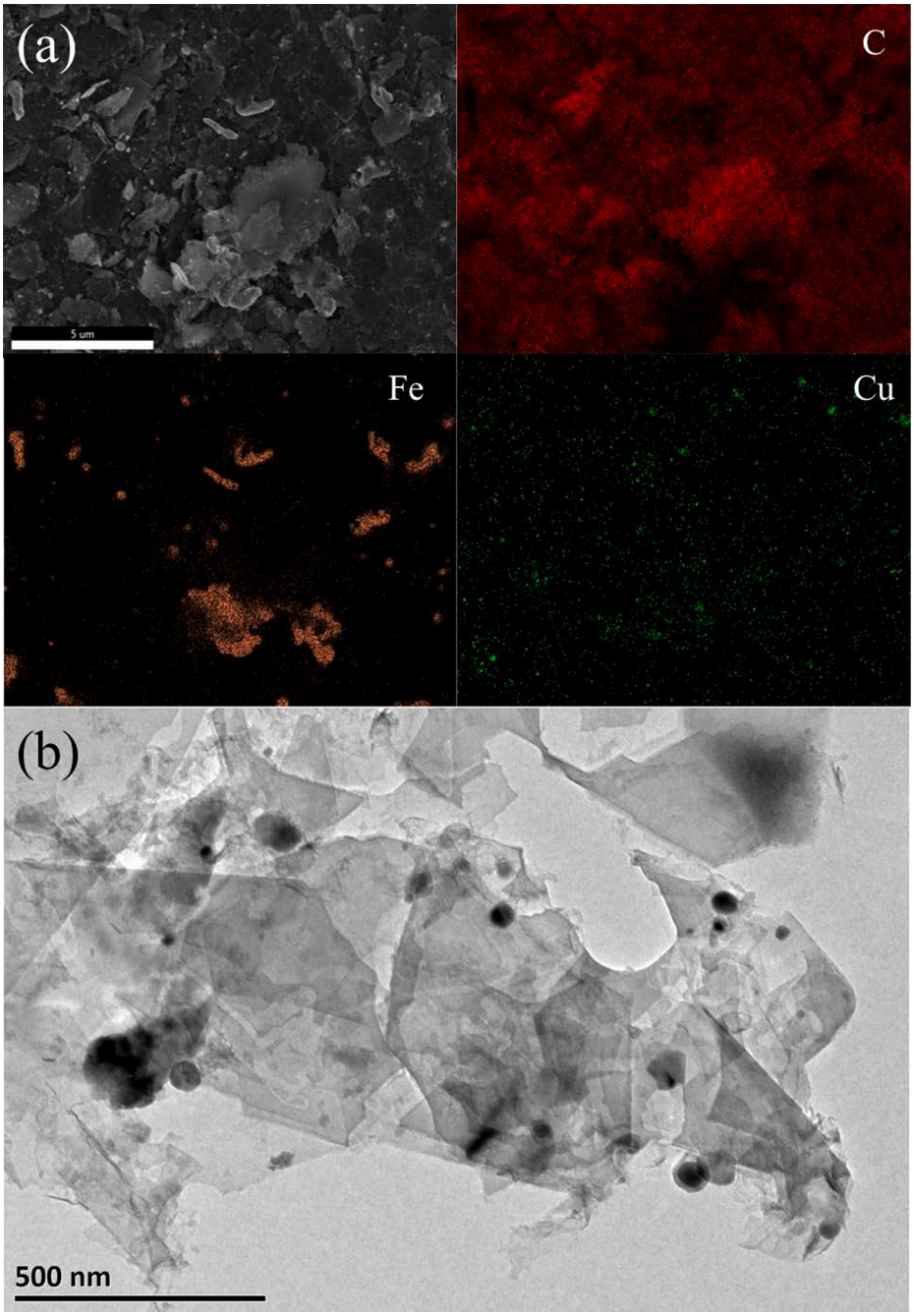

Fig. 3. (a) SEM- EDS and (b) TEM images of ZVI-Cu/C-2.

beam [42]. The peaks of iron oxide species at about 713 and 725 eV can also be found in this figure. The C 1s deconvoluted spectrum shows two peaks, a main one centered at 284.9 eV and another smaller at 286.8 eV that can be related to the presence of C-C and C-O in graphite, respectively [43]. The Cu 2p spectrum shows peaks centered at 932.5 and 952.6 eV for zerovalent metallic copper, as well as smaller peaks cooper oxide species [44].

The surface elemental composition of the ZVI-Cu/C catalysts obtained from XPS is shown in Table 2. The increase of the MS dosage results in an expected increase of iron content, and reduction of the carbon proportion. This is due to a double effect. First, the higher MS amount comes with a lower graphite proportion and second, more graphite is consumed in the reduction reaction due to the higher amount of Fe from MS, in agreement with the XRD results. In addition, the copper content remains almost stable, confirming that there is no loss of copper during the carbothermal reduction reaction. Despite the increase in the MS proportion was expected to decrease the Cu proportion, the significant loss of graphite during the carbothermal reaction seems to compensate this reduction, resulting in an almost constant Cu content regardless of the MS to LIBs mass ratio. The BET surface area of the ZVI-Cu/C catalysts is summarized in Table 2. All of them have very low surface areas (<2 m^2/g) characteristic of non-porous materials. These low area values do not prevent the catalysts from showing significant activity in both oxidation and reduction reactions.

3.3. Degradation of 4-CP in water

The degradation of 4-CP by different ZVI-Cu/C catalysts through heterogeneous Fenton reaction (in the presence of H_2O_2) is shown in Fig. 5a. The final removal percentage after 2 h was 79% when using ZVI-

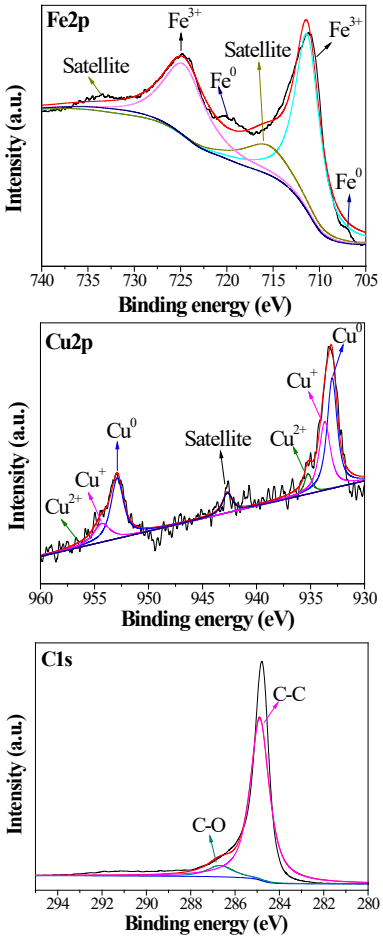

Fig. 4. XPS results of ZVI-Cu/C-2 catalyst.

Table 2
Elemental surface concentration by EDS and BET surface area.

Element	ZVI-Cu/C-1	ZVI-Cu/C-2	ZVI-Cu/C-3	ZVI-Cu/C-4
C (wt%)	84.8	74.0	24.4	20.8
Fe (wt%)	5.9	13.0	51.1	64.0
Cu (wt%)	1.2	0.5	0.4	0.7
BET surface area (m^2/g)	1.7	1.8	1.7	1.1

Cu/C-1, and total degradation of 100% was achieved with ZVI-Cu/C-2. This is probably because the higher ZVI amount of iron in ZVI-Cu/C-2, resulting in more available Fe^{2+} and thus higher amount of •OH radicals for the oxidation of 4-CP in water [45]. However, when ZVI-Cu/C-3 and ZVI-Cu/C-4 were used, the removal percentage of 4-CP decreased very significantly, being 52% for ZVI-Cu/C-4, and even lower for ZVI-Cu/C-1. This may be due to the much higher amount of Fe^{2+} in these catalysts, which can compete with 4-CP reducing the •OH available involved in the degradation reaction [46]. Furthermore, the very high amount of iron can also result in a very fast H_2O_2 decomposition, which decrease the overall efficiency of the process [47].

The oxidation of 4-CP by ZVI-Cu/C can be fitted to a pseudo-first order kinetic model, as depicted in Fig. 5b. The pseudo-first order rate constants are shown in Table 3. The removal rate of ZVI-Cu/C-2 reaches 0.028 min^{-1}, higher than 0.00008 min^{-1} by using Fe(II) and H_2O_2 reported by Jin et al. [48], and the 0.016 min^{-1} obtained with mesoporous carbon activated with peroxydisulfate reported by Yang et al. [49]. The XRD results of ZVI-Cu/C-2 after reaction are shown in Fig. 6. The comparison of the XRD pattern with that of the non-used ZVI-Cu/C-2

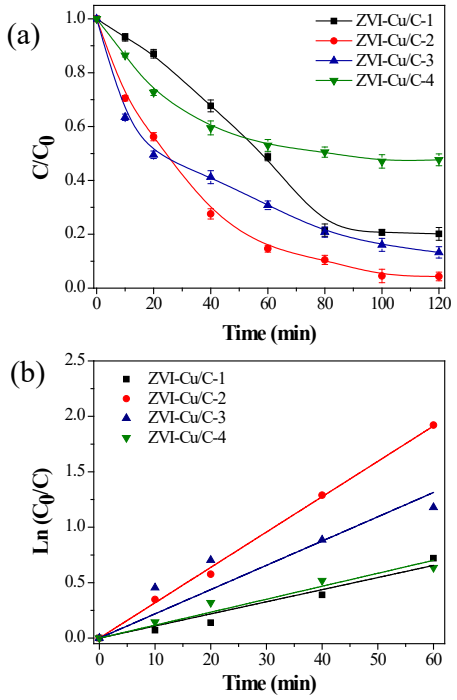

Fig. 5. (a) 4-CP removal performances of ZVI-Cu/C composites in heterogeneous Fenton system, (b) fitting results of pseudo-first order kinetic model.

Table 3
Fitting results of pseudo-first order reaction kinetics of different ZVI-Cu/C composites.

ZVI-Cu/C composites	Heterogeneous Fenton		Reduction	
	k (min^{-1})	R^2	k (h^{-1})	R^2
ZVI-Cu/C-1	0.016	0.917	0.096	0.977
ZVI-Cu/C-2	0.028	0.957	0.244	0.999
ZVI-Cu/C-3	0.016	0.966	0.034	0.996
ZVI-Cu/C-4	0.006	0.837	0.022	0.998

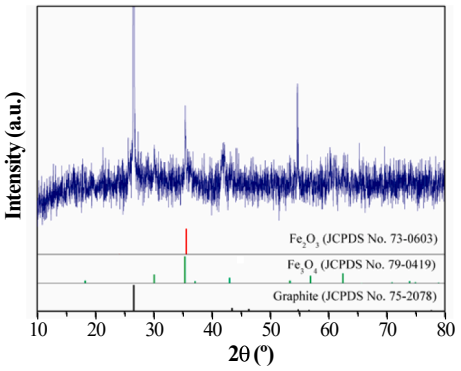

Fig. 6. XRD results of ZVI-Cu/C-2 after reaction.

shows the transformation of the catalyst's surface into Fe_2O_3 (JCPDS No. 73–0603) and Fe_3O_4 (JCPDS No. 79–0419) as a consequence of the oxidation of the ZVI during the reaction. The evolution of iron and copper ions content in water during reaction with ZVI-Cu/C-2 is summarized in Table 4. The final concentration of iron and copper ions reached 6.980 and 0.002 mg/L, respectively. As can be seen in the table, the metal lixiviation seems to happen only at the beginning of the reaction, after that almost no additional leaching is produced. Probably, the iron oxides generated on the graphite surface during the oxidation

Table 4
Concentrations of iron and copper ions in solution at different time.

Heterogeneous Fenton system	Time (min)	10	20	40	60	80	100
	Fe ion(mg/L)	1.28	2.70	5.46	5.56	6.46	6.98
	Cu ion(mg/L)	0.002	0.002	0.006	0.006	0.004	0.002
Reduction system	Time (h)	1	2	3	4	5	6
	Fe ion(mg/L)	14.04	15.02	15.08	15.18	15.16	15.24
	Cu ion(mg/L)	0.042	0.064	0.06	0.056	0.062	0.054

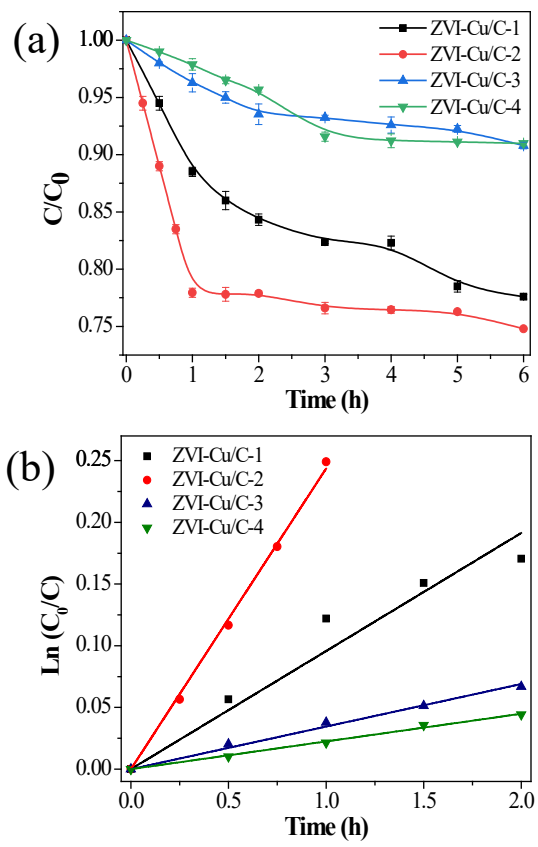

Fig. 7. (a) 4-CP removal performances of ZVI-Cu/C composites in reduction system, (b) fitting results of pseudo-first order kinetic model.

reaction avoid an excessive iron loss in water.

In the case of the reduction tests (without H_2O_2), the removal percentages of 4-CP by ZVI-Cu/C materials were 22.5 and 25.2% when using ZVI-Cu/C-1 and ZVI-Cu/C-2, respectively (Fig. 7a). The conversion values decreased approximately 10% with ZVI-Cu/C-3 and ZVI-Cu/C-4 catalysts. The reduction of 4-CP by ZVI-Cu/C composites fits also well a pseudo-first order kinetic model, as shown in Fig. 7b. The pseudo-first order rate constants are included in Table 3, which are much lower than those obtained in the heterogeneous Fenton reaction. ZVI-Cu/C-2 shows better 4-CP removal performance than ZVI-Cu/C-1, due to the higher Fe (ZVI) content as showed in Table 2. Although in ZVI-Cu/C-3 and ZVI-Cu/C-4 the amount of ZVI increased, it is likely that these high iron contents resulted in the agglomeration of ZVI, which reduced the reactivity of ZVI-Cu/C, resulting in the observed decrease in the removal rate. The evolution of the concentrations of iron and copper ions in the water during reduction reaction are shown in Table 4. Concentrations of ions in the reduction system are significantly higher than those in the heterogeneous Fenton system, which is in the agreement with the higher stability of the iron oxides species formed in the heterogeneous Fenton reaction. These results show that 4-CP can be degraded by ZVI-Cu/C catalysts by both reduction and oxidation reactions [43,50,51], although the oxidation reactions show a markedly higher activity. The reactions during the removal of 4-CP by ZVI-Cu/C composites are described by Eqs. 4–15 [27,52,53].

$$Fe^0 + 2H^+ \rightarrow Fe^{2+} + H_2\uparrow \quad (4)$$

$$2Fe^0 + O_2 + 2H_2O \rightarrow 2Fe^{2+} + 4OH^- \quad (5)$$

$$Fe^0 + O_2 + 2H^+ \rightarrow Fe^{2+} + H_2O_2 \quad (6)$$

$$Fe^{2+} + H_2O_2 \rightarrow Fe^{3+} + OH + OH^- \quad (7)$$

$$Fe^{3+} + H_2O_2 \rightarrow Fe^{2+} + O_2H + H^+ \quad (8)$$

$$2Cu^0 + 2H^+ \rightarrow 2Cu^+ + H_2\uparrow \quad (9)$$

$$Cu_2O + 2H+ \rightarrow 2Cu^+ + H_2O \quad (10)$$

$$4Cu^+ + 4H^+ + O_2 \rightarrow 4Cu^{2+} + 2H_2O \quad (11)$$

$$Cu^+ + H2O2 \rightarrow Cu^{2+} + OH + OH^- \quad (12)$$

$$Cu^{2+} + H2O2 \rightarrow Cu^+ + O_2H + H^+ \quad (13)$$

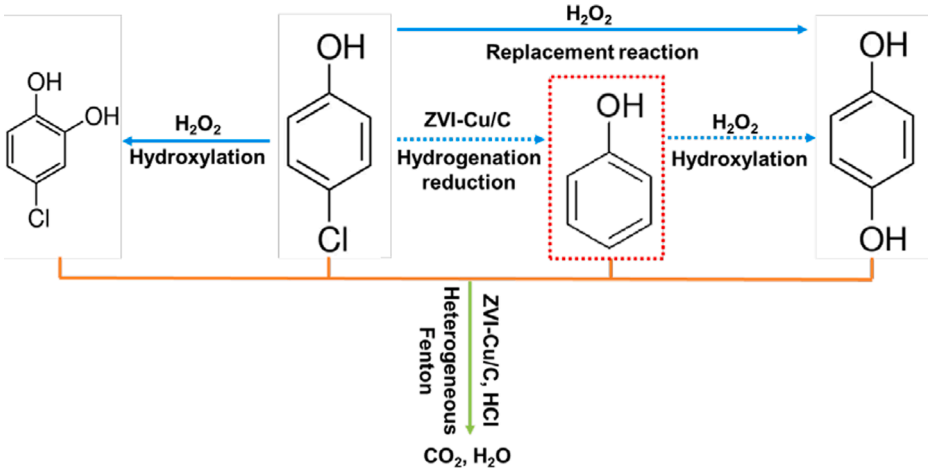

Fig. 8. Possible degradation mechanism of 4-CP.

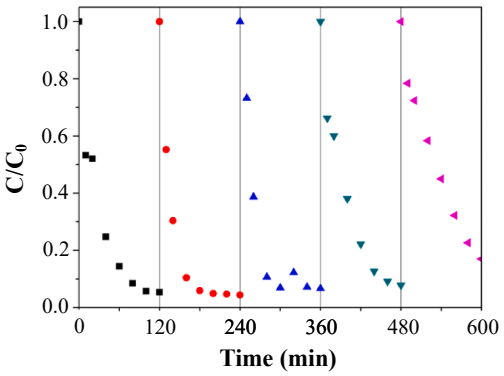

Fig. 9. Reuse performance of ZVI-Cu/C-2 for 4-CP removal.

$$Cu^{2+}+O_2H \rightarrow Cu^{+}+H^{+}+O_2 \quad (14)$$

$$Fe^{0}+Cu^{2+}\rightarrow Cu^{0}+Fe^{2+} \quad (15)$$

The oxidation degradation mechanism of 4-CP was further studied by using GC–MS to detect the reaction by-products. Fig. 8 depicts a proposed 4-CP degradation pathway. Two compounds, 4-chlorocatechol and hydroquinone, were determined as intermediate products of 4-CP degradation. The 4-chlorocatechol was formed through the hydroxylation of 4-CP, while hydroquinone was formed through the replacement reaction or might be formed from the hydroxylation of phenol, which may produce from the hydroxylation of hydrogenation reduction of 4-CP [54–56]. These compounds will be then degraded to form carbon dioxide and water [48].

The stability of ZVI-Cu/C-2 in heterogeneous Fenton reactions is studied by the analysis of the 4-CP removal percentage in different cycles, as showed in Fig. 9. 4-CP conversion was still high even in the fourth cycle (92.1%), although a significant decrease in conversion is observed in the fifth cycle. Table 5 lists the removal percentages of 4-CP and the main reaction conditions reported in literature using different technologies and catalysts. The data indicate that the ZVI-Cu/C catalysts synthesized in this study show competitive removal of 4-CP in relation with those previous studies using methods of oxidation, reduction, biological degradation, photocatalytic degradation and heterogeneous Fenton. Among these methods, biological treatment has the characteristics of low cost and no pollution, but the reaction time is usually much longer, because the time needed to cultivate the microorganisms with degradation ability [36]. Further, the reduction method can just dechlorinate of 4-CP, generating intermediate products like phenol and phenol-derivates that still need to be treated [28]. Oxidation, Photocatalytic degradation, and heterogeneous Fenton processes can totally degrade 4-CP to form CO_2 and H_2O in a shorter period of time, but finding catalysts which are easy to fabricate, and cost effective is essential [38]. In this way, catalysts fabricated with recycled materials are good candidates for the use for 4-CP removal in water.

4. Conclusions

ZVI-Cu/C catalysts with high activity for 4-CP degradation were synthesized. The copper and graphite content was obtained from spent LIB anode, while iron oxide was obtained from MS waste. The catalysts were prepared by a simple and straightfoward carbothermic reduction process. ZVI-Cu/C-2 showed the best 4-CP removal performances in both reduction and heterogeneous Fenton systems. The iron and copper leached to the water is relatively low in the heterogeneous Fenton system (and observed only at the fisrt stages of the reactions), which supports the good stability of the synthesized materilals and decrease the risks of potential impacts on the environment. Two reaction by-products, 4-chlorocatechol and hydroquinone, were identified in the 4-CP degradation by the Fenton reaction. This study confirms the possibility of recycling spent LIB anode and MS to synthesize active and stable ZVI-Cu/C catalysys for the removal of pollutants from water using different types of degradation reactions, such as oxidation or reduction.

Declaration of Competing Interest

The authors declare that they have no known competing financial interests or personal relationships that could have appeared to influence

Table 5
4-CP removal by various techniques.

Catalyst	Removal percentage	Method	Condition	Ref.
zero valent mono/bimetallic catalyst	100%	Reduction	15 mg·L^{-1} 4-CP, 3 g·L^{-1} zero valent mono/bimetallic catalysts, 4 h	[28]
nZVI-Ni	96%	Reduction	64 mg·L^{-1} 4-CP, 2 g·L^{-1} nZVI-Ni, 120 min	[29]
ZVI-mellitic acid	80%	Oxidation	13 mg·L^{-1} 4-CP, 0.2 g·L^{-1} ZVI, 10 mM benzoic acid, 120 min	[30]
ultrasound/peroxymonosulfate/nZVI	95%	Oxidation	0.4 g·L^{-1} nZVI, 1.2524 mM PMS, 200 W US power, 30 min	[31]
Needle-net PHVD reactor	86.2%	Oxidation	100 mg·L^{-1} 4-CP, air flux 200 mL·min^{-1}, discharge voltage 20 kV, frequency 100 Hz, solution conductivity 116 μS·cm^{-1}, 40 min	[32]
Phosphomolybdic acid/H_2O_2	100%	Oxidation	0.778 mM 4-CP, 3.89 mM phosphomolybdic acid, pH 3, 90 °C, H_2O_2 156 mM, 60 min	[33]
La/TiO_2/dielectric barrier discharge system	99.9%	Oxidation	100 mg L-1 4-CP, pH 10, 100 W	[34]
Hydrogen-based membrane biofilm reactor	100%	Biological elimination	100 mg·L^{-1} 4-CP, flow rate 1 mL·min^{-1}	[35]
Bacillus flexus	90.34	Biological elimination	1.2107 CFU·mL^{-1} bacterial inoculums, 30 °C, 50 mg·L^{-1} 4-CP, 7 days	[36]
NbO-400/GR composites	94%	Photocatalytic degradation	1 g·L^{-1} NbO/GR composites, 20 mg·L^{-1} 4-CP, 300 W Xenon lamp, 5 h	[37]
RPS-CuST	100%	Photocatalytic degradation	1 g·L^{-1} RPS-CuST, 20 mg·L^{-1} 4-CP, 75 W Xenon lamp, 5 h	[38]
TiO_2 nanocone	99%	Photocatalytic degradation	20 mg·L^{-1} 4-CP, 3 h, pH 5.67, 300 Wxenon lamp	[39]
Iron-glutamate-silicotungstate ternary complex	100%	Heterogeneous Fenton	4-CP 100 mg·L^{-1},FeIIIGluSiW 1.0 g·L^{-1}, H_2O_2 20 mmol·L^{-1}, 40 min	[40]
iron-containing silicotungstate	100%	Heterogeneous Fenton	100 mg·L^{-1} 4-CP, 0.2 g·L^{-1} iron-containing silicotungstate, 20 mM H_2O_2, 30 min	[41]
ZVI-Cu/C	100%	Heterogeneous Fenton	10 mg·L^{-1} 4-CP, 0.2 g·L^{-1} ZVI-Cu/C-2, 0.5 mM H_2O_2, 120 min	This study

the work reported in this paper.

Acknowledgements

This work was supported by China Scholarship Council (202008310005), National Natural Science Foundation of China (52070127), Science and Technology Commission of Shanghai Municipality (21WZ2501500).

References

[1] J. Ordoñez, E.J. Gago, A. Girard, Processes and technologies for the recycling and recovery of spent lithium-ion batteries, Renew. Sust. Energ. Rev. 60 (2016) 195–205, https://doi.org/10.1016/j.rser.2015.12.363.
[2] G. Harper, R. Sommerville, E. Kendrick, L. Driscoll, P. Slater, R. Stolkin, A. Walton, P. Christensen, O. Heidrich, S. Lambert, A. Abbott, K. Ryder, L. Gaines, P. Anderson, Recycling lithium-ion batteries from electric vehicles, Nature 575 (7781) (2019) 75–86, https://doi.org/10.1038/s41586-019-1682-5.
[3] M.M. Thackeray, C. Wolverton, E.D. Isaacs, Electrical energy storage for transportation-approaching the limits of, and going beyond, lithium-ion batteries, Energy Environ. Sci. 5 (2012) 7854–7863, https://doi.org/10.1039/C2EE21892E.
[4] B. Swain, Cost effective recovery of lithium from lithium ion battery by reverse osmosis and precipitation: A perspective, J. Chem. Technol. Biot. 93 (2) (2018) 311–319, https://doi.org/10.1002/jctb.5332.
[5] W. Lv, Z. Wang, H. Cao, Y. Sun, Y.i. Zhang, Z. Sun, A critical review and analysis on the recycling of spent lithium-ion batteries, ACS Sust. Chem. Eng. 6 (2) (2018) 1504–1521, https://doi.org/10.1021/acssuschemeng.7b03811.
[6] X. Zeng, J. Li, N. Singh, Recycling of spent lithium-ion battery: A critical review, Crit. Rev. Env. Sci. Tec. 44 (10) (2014) 1129–1165, https://doi.org/10.1080/10643389.2013.763578.
[7] W. Yan, H. Cao, Y.i. Zhang, P. Ning, Q. Song, J. Yang, Z. Sun, Rethinking Chinese supply resilience of critical metals in lithium-ion batteries, J. Cleaner Prod. 256 (2020) 120719, https://doi.org/10.1016/j.jclepro.2020.120719.
[8] N. Vieceli, R. Casasola, G. Lombardo, B. Ebin, M. Petranikova, Hydrometallurgical recycling of EV lithium-ion batteries: Effects of incineration on the leaching efficiency of metals using sulfuric acid, Waste Manage. 125 (2021) 192–203, https://doi.org/10.1016/j.wasman.2021.02.039.
[9] B.o. Niu, J. Xiao, Z. Xu, Utilizing spent Li-ion batteries to regulate the π-conjugated structure of g-C_3N_4: A win–win approach for waste recycling and highly active photocatalyst construction, J. Mater. Chem. A 9 (1) (2021) 472–481, https://doi.org/10.1039/D0TA10881B.
[10] J. Liang, Y. Xue, J.-N. Gu, J. Li, F. Shi, X. Guo, M. Guo, X. Min, K. Li, T. Sun, J. Jia, Sustainably recycling spent lithium-ion batteries to prepare magnetically separable cobalt ferrite for catalytic degradation of bisphenol A via peroxymonosulfate activation, J. Hazard. Mater. (2021) 127910, https://doi.org/10.1016/j.jhazmat.2021.127910.
[11] Y. Zhao, X. Yuan, L. Jiang, X. Li, J. Zhang, H. Wang, Reutilization of cathode material from spent batteries as a heterogeneous catalyst to remove antibiotics in wastewater via peroxymonosulfate activation, Chem. Eng. J. 400 (2020) 125903, https://doi.org/10.1016/j.cej.2020.125903.
[12] Y. Zhang, Y. Wang, H. Zhang, Y. Li, Z. Zhang, W. Zhang, Recycling spent lithium-ion battery as adsorbents to remove aqueous heavy metals: Adsorption kinetics, isotherms, and regeneration assessment, Res. Conser. Recy. 156 (2020) 104688, https://doi.org/10.1016/j.resconrec.2020.104688.
[13] K. Sivagami, K. Padmanabhan, A.C. Joy, I.M. Nambi, Microwave (MW) remediation of hydrocarbon contaminated soil using spent graphite - An approach for waste as a resource, J. Environ. Manage. 230 (2019) 151–158, https://doi.org/10.1016/j.jenvman.2018.08.071.
[14] N. Gade, G. Verma, R. Sen, U. Pandel, Effect of calcium carbonate on the reduction behaviour of mill scale, Proc. Earth Planet. Sci. 11 (2015) 319–324, https://doi.org/10.1016/j.proeps.2015.06.067.
[15] S. Cho, J. Lee, Metal recovery from stainless steel mill scale by microwave heating, Met. Mater. Int. 14 (2008) 193–196, https://doi.org/10.3365/met.mat.2008.04.193.
[16] G. Bantsis, M. Betsiou, A. Bourliva, T. Yioultsis, C. Sikalidis, Synthesis of porous iron oxide ceramics using greek wooden templates and mill scale waste for emi applications, Ceram. Int. 38 (1) (2012) 721–729, https://doi.org/10.1016/j.ceramint.2011.07.064.
[17] M.K. Shahid, S. Phearom, Y.-G. Choi, Synthesis of magnetite from raw mill scale and its application for arsenate adsorption from contaminated water, Chemosphere 203 (2018) 90–95, https://doi.org/10.1016/j.chemosphere.2018.03.150.
[18] B. Liu, L.i. Zhang, Y. Zhang, G. Han, B. Zhang, Innovative methodology for co-treatment of mill scale scrap and manganese ore via oxidization roasting-magnetic separation for preparation of ferrite materials, Ceram. Int. 47 (5) (2021) 6139–6153, https://doi.org/10.1016/j.ceramint.2020.10.193.
[19] P.C. Jikar, N.B. Dhokey, Influence of process parameters on countercurrent reactor reduction of oxidized mill scale waste and its co-relationship with mathematical model, J. Sustain. Metall. 6 (4) (2020) 622–630, https://doi.org/10.1007/s40831-020-00297-0.
[20] Y. Sun, J. Li, T. Huang, X. Guan, The influences of iron characteristics, operating conditions and solution chemistry on contaminants removal by zero-valent iron: A review, Water Res. 100 (2016) 277–295, https://doi.org/10.1016/j.watres.2016.05.031.
[21] B. Flury, J. Frommer, U. Eggenberger, U. Mäder, M. Nachtegaal, R. Kretzschmar, Assessment of long-term performance and chromate reduction mechanisms in a field scale permeable reactive barrier, Environ. Sci. Technol. 43 (17) (2009) 6786–6792, https://doi.org/10.1021/es803526g.
[22] Y. Yu, Z. Huang, D. Deng, Y. Ju, L. Ren, M. Xiang, L. Li, H. Li, Synthesis of millimeter-scale sponge Fe/Cu bimetallic particles removing tbbpa and insights of degradation mechanism, Chem. Eng. J. 325 (2017) 279–288, https://doi.org/10.1016/j.cej.2017.05.018.
[23] Z. Xu, X. Xu, Y. Zhang, Y. Yu, X. Cao, Pyrolysis-temperature depended electron donating and mediating mechanisms of biochar for Cr(VI) reduction, J. Hazard. Mater. 388 (2020) 121794, https://doi.org/10.1016/j.jhazmat.2019.121794.
[24] Y.M.Z. Ahmed, M.M. Hessien, M.M. Rashad, I.A. Ibrahim, Nano-crystalline copper ferrites from secondary iron oxide (mill scale), J. Magn. Magn. Mater. 321 (3) (2009) 181–187, https://doi.org/10.1016/j.jmmm.2008.08.100.
[25] J. Liang, X. Duan, X. Xu, K. Chen, F. Wu, H. Qiu, C. Liu, S. Wang, X. Cao, Biomass-derived pyrolytic carbons accelerated Fe(III)/Fe(II) redox cycle for persulfate activation: Pyrolysis temperature-depended performance and mechanisms, Appl. Catal. B-Environ. 297 (2021) 120446, https://doi.org/10.1016/j.apcatb.2021.120446.
[26] F.-D. Kopinke, S. Sühnholz, A. Georgi, K. Mackenzie, Interaction of zero-valent iron and carbonaceous materials for reduction of DDT, Chemosphere 253 (2020) 126712, https://doi.org/10.1016/j.chemosphere.2020.126712.
[27] S. Chen, Z. Li, C. Belver, G. Gao, J. Guan, Y. Guo, H. Li, J. Ma, J. Bedia, P. Wójtowicz, Comparison of the behavior of zvi/carbon composites from both commercial origin and from spent li-ion batteries and mill scale for the removal of ibuprofen in water, J. Environ. Manage. 264 (2020) 110480, https://doi.org/10.1016/j.jenvman.2020.110480.
[28] S.S. Raut, R. Shetty, N.M. Raju, S.P. Kamble, P.S. Kulkarni, Screening of zero valent mono/bimetallic catalysts and recommendation of raney ni (without reducing agent) for dechlorination of 4-chlorophenol, Chemosphere 250 (2020) 126298, https://doi.org/10.1016/j.chemosphere.2020.126298.
[29] Y. Hwang, P.D. Mines, M.H. Jakobsen, H.R. Andersen, Simple colorimetric assay for dehalogenation reactivity of nanoscale zero-valent iron using 4-chlorophenol, Appl. Catal. B-Environ. 166–167 (2015) 18–24, https://doi.org/10.1016/j.apcatb.2014.10.059.
[30] S.H. Kang, A.D. Bokare, Y. Park, C.H. Choi, W. Choi, Electron shuttling catalytic effect of mellitic acid in zero-valent iron induced oxidative degradation, Catal. Today 282 (2017) 65–70, https://doi.org/S092058611630178X.
[31] G. Barzegar, S. Jorfi, V. Zarezade, M. Khatebasreh, F. Mehdipour, F. Ghanbari, 4-chlorophenol degradation using ultrasound/peroxymonosulfate/nanoscale zero valent iron: Reusability, identification of degradation intermediates and potential application for real wastewater, Chemosphere 201 (2018) 370–379, https://doi.org/10.1016/j.chemosphere.2018.02.143.
[32] Y. Su, S. Liu, C. Zhao, X. Yang, L. Huang, X. Peng, D. Liu, Needle electrode design of pulsed high voltage discharge reactor for performance enhancement of 4-chlorophenol degradation in highly conductive solution, Chemosphere 266 (2021) 129203, https://doi.org/10.1016/j.chemosphere.2020.129203.
[33] M. Lei, Q. Gao, K. Zhou, P. Gogoi, J. Liu, J. Wang, H. Song, S. Wang, X. Liu, Catalytic degradation and mineralization mechanism of 4-chlorophenol oxidized by phosphomolybdic acid/H_2O_2, Sep. Purif. Technol. 257 (2021) 117933, https://doi.org/10.1016/j.seppur.2020.117933.
[34] S. Li, Y. Xu, X. Wang, Y. Guo, Q. Mu, Catalytic degradation of 4-chlorophenol with La/TiO_2 in a dielectric barrier discharge system, RSC Adv. 6 (34) (2016) 28994–29002, https://doi.org/10.1039/C6RA02807A.
[35] M. Long, C. Zeng, Z. Wang, S. Xia, C. Zhou, Complete dechlorination and mineralization of para-chlorophenol (4-CP) in a hydrogen-based membrane biofilm reactor (mbfr), J. Clean. Prod. 276 (2020) 123257, https://doi.org/10.1016/j.jclepro.2020.123257.
[36] G. Swain, R.K. Sonwani, R.S. Singh, R.P. Jaiswal, B.N. Rai, Removal of 4-chlorophenol by bacillus flexus as free and immobilized system: Effect of process variables and kinetic study, Environ. Technol. Inno. 21 (2021) 101356, https://doi.org/10.1016/j.eti.2021.101356.
[37] J. Yang, J. Hao, S. Xu, J. Dai, Y. Wang, X. Pang, Visible-light-driven photocatalytic degradation of 4-CP and the synergistic reduction of Cr(VI) on one-pot synthesized amorphous Nb_2O_5 nanorods/graphene heterostructured composites, Chem. Eng. J. 353 (2018) 100–114, https://doi.org/10.1016/j.cej.2018.07.115.
[38] E. Valadez-Renteria, E. Barrera-Rendon, J. Oliva, V. Rodriguez-Gonzalez, Flexible CuS/TiO_2 based composites made with recycled bags and polystyrene for the efficient removal of the 4-CP pesticide from drinking water, Sep. Purif. Technol. 270 (2021) 118821, https://doi.org/10.1016/j.seppur.2021.118821.
[39] R. Song, H. Chi, Q. Ma, D. Li, X. Wang, W. Gao, H. Wang, X. Wang, Z. Li, C. Li, Highly efficient degradation of persistent pollutants with 3D nanocone TiO_2-based photoelectrocatalysis, J. Am. Chem. Soc. 143 (34) (2021) 13664–13674, https://doi.org/10.1021/jacs.1c0500810.1021/jacs.1c05008.s001.
[40] D. Yin, L. Zhang, X. Zhao, H. Chen, Q. Zhai, Iron-glutamate-silicotungstate ternary complex as highly active heterogeneous fenton-like catalyst for 4-chlorophenol degradation, Chinese, J. Catal. 36 (12) (2015) 2203–2210, https://doi.org/10.1016/S1872-2067(15)61011-7.
[41] H. Chen, L. Zhang, H. Zeng, D. Yin, Q. Zhai, X. Zhao, J. Li, Highly active iron-containing silicotungstate catalyst for heterogeneous fenton oxidation of 4-chlorophenol, J. Mol. Catal. A: Chem. 406 (2015) 72–77, https://doi.org/10.1016/j.molcata.2015.05.017.
[42] Y. Li, Z. Jin, T. Li, Z. Xiu, One-step synthesis and characterization of core–shell Fe@SiO_2 nanocomposite for Cr(VI) reduction, Sci. Total Environ. 421–422 (2012) 260–266, https://doi.org/10.1016/j.scitotenv.2012.01.010.

[43] L. Xu, Y. Yang, W. Li, Y. Tao, Z. Sui, S. Song, J. Yang, Three-dimensional macroporous graphene-wrapped zero-valent copper nanoparticles as efficient micro-electrolysis-promoted fenton-like catalysts for metronidazole removal, Sci. Total Environ. 658 (2019) 219–233, https://doi.org/10.1016/j.scitotenv.2018.12.040.

[44] T. Zhang, Y. Yang, X. Li, H. Yu, N. Wang, H. Li, P. Du, Y. Jiang, X. Fan, Z. Zhou, Degradation of sulfamethazine by persulfate activated with nanosized zero-valent copper in combination with ultrasonic irradiation, Sep. Purif. Technol. 239 (2020) 116537, https://doi.org/10.1016/j.seppur.2020.116537.

[45] L. Xu, J. Wang, A heterogeneous fenton-like system with nanoparticulate zero-valent iron for removal of 4-chloro-3-methyl phenol, J. Hazard. Mater. 186 (1) (2011) 256–264, https://doi.org/10.1016/j.jhazmat.2010.10.116.

[46] C. Liu, Y. Liu, Z. Dang, S. Zeng, C. Li, Enhancement of heterogeneous photo-fenton performance of core-shell structured boron-doped reduced graphene oxide wrapped magnetical Fe_3O_4 nanoparticles: Fe(II)/Fe(III) redox and mechanism, Appl. Surf. Sci. 544 (2021) 148886, https://doi.org/10.1016/j.apsusc.2020.148886.

[47] J. Bedia, V.M. Monsalvo, J.J. Rodriguez, A.F. Mohedano, Iron catalysts by chemical activation of sewage sludge with $FeCl_3$ for CWPO, Chem. Eng. J. 318 (2017) 224–230, https://doi.org/10.1016/j.cej.2016.06.096.

[48] Q. Jin, Q. Chen, J. Shen, F. Guo, Z. Chen, J. Tian, Development of Fe(II) system based on N, N'-dipicolinamide for the oxidative removal of 4-chlorophenol, J. Hazard. Mater. 354 (2018) 206–214, https://doi.org/10.1016/j.jhazmat.2018.04.058.

[49] J. Yang, X. He, J. Dai, Y. Chen, Y. Li, X. Hu, Electron-transfer-dominated non-radical activation of peroxydisulfate for efficient removal of chlorophenol contaminants by one-pot synthesized nitrogen and sulfur codoped mesoporous carbon, Environ. Res. 194 (2021) 110496, https://doi.org/10.1016/j.envres.2020.110496.

[50] G. Wen, S.-J. Wang, J. Ma, T.-L. Huang, Z.-Q. Liu, L. Zhao, J.-L. Xu, Oxidative degradation of organic pollutants in aqueous solution using zero valent copper under aerobic atmosphere condition, J. Hazard. Mater. 275 (2014) 193–199, https://doi.org/10.1016/j.jhazmat.2014.05.002.

[51] X. Lai, X.-A. Ning, Y. He, Y. Yuan, J. Sun, Y. Ke, X. Man, Treatment of a simulated sludge by ultrasonic zero-valent iron/edta/air process: Interferences of inorganic salts in polyaromatic hydrocarbon removal, Waste Manage. 85 (2019) 548–556, https://doi.org/10.1016/j.wasman.2019.01.009.

[52] J.-H. Chu, J.-K. Kang, S.-J. Park, C.-G. Lee, Bisphenol a degradation using waste antivirus copper film with enhanced sono-Fenton-like catalytic oxidation, Chemosphere 276 (2021) 130218, https://doi.org/10.1016/j.chemosphere.2021.130218.

[53] L.i. Zhang, Y. Fu, Z. Wang, G. Zhou, R. Zhou, Y. Liu, Removal of diclofenac in water using peracetic acid activated by zero valent copper, Sep. Purif. Technol. 276 (2021) 119319, https://doi.org/10.1016/j.seppur.2021.119319.

[54] G. Vega, A. Quintanilla, M. Belmonte, J.A. Casas, Kinetic study of phenol hydroxylation by H_2O_2 in 3D Fe/SiC honeycomb monolithic reactors: Enabling the sustainable production of dihydroxybenzenes, Chem. Eng. J. 428 (2022) 131128, https://doi.org/10.1016/j.cej.2021.131128.

[55] S. Mishra, R. Bal, R.K. Dey, Heterogeneous recyclable copper oxide supported on activated red mud as an efficient and stable catalyst for the one pot hydroxylation of benzene to phenol, Mol. Catal. 499 (2021) 111310, https://doi.org/10.1016/j.mcat.2020.111310.

[56] K. Anjali, V. Ganesh, J. Christopher, A. Sakthivel, Copper based macromolecular catalysts for the hydroxylation of phenols, J. Organomet. Chem. 929 (2020) 121579, https://doi.org/10.1016/j.jorganchem.2020.121579.